

## REGIONAL AND HISTORICAL GEOCRYOLOGY

FORMATION OF THE HOLLOW-RIDGE TOPOGRAPHY  
ON THE PUR–TAZ INTERFLUVE IN THE LATE PLEISTOCENE AND HOLOCENEO.L. Opokina<sup>1,2,\*</sup>, E.A. Slogoda<sup>1,2</sup>, V.I. Ivanov<sup>1</sup>, A.V. Khomutov<sup>1</sup>, A.O. Kuznetsova<sup>1</sup>,  
M.M. Danko<sup>1</sup>, E.S. Koroleva<sup>3</sup>, G.V. Simonova<sup>4</sup><sup>1</sup> Institute of Earth Cryosphere, Malygina St. 8, Tyumen, 625026 Russia<sup>2</sup> Tyumen Industrial University, Volodarskogo St. 38, Tyumen, 625000 Russia<sup>3</sup> Arctic Research Center of the Yamal-Nenets Autonomous Okrug, Respubliki St. 20, Salekhard, 629008 Russia<sup>4</sup> Institute of Monitoring of Climatic and Ecological Systems, Akademicheskii prosp. 10/3, Tomsk, 634055 Russia

\*Corresponding author; e-mail: opokina@ikz.ru

The structure of the upper part of permafrost and the topographic features in the northeast of Western Siberia were shaped by changes in the natural environment in the Late Pleistocene and Holocene. In 2016–2021, sections of different landforms – ridges and thermokarst-erosional hollows – were studied within the third lacustrine-alluvial plain of the Pur–Taz interfluvium. The upper part of the plain includes the Kargin–Sartan alluvial, lacustrine, and slope sediments and Holocene peatlands. Based on the stratigraphy and new geochronological data on the Pur–Taz interfluvium, the consequences of the activation of neotectonic processes in the Sartan period and the influence of climatic factors on the differentiation of accumulative and denudation processes in the Holocene were identified.

**Keywords:** cryogenic structure, genesis of sediment, peatlands, radiocarbon dating, relief, neotectonics.

**Recommended citation:** Opokina O.L., Slogoda E.A., Ivanov V.I., Khomutov A.V., Kuznetsova A.O., Danko M.M., Koroleva E.S., Simonova G.V., 2024. Formation of the hollow-ridge topography on the Pur–Taz interfluvium in the Late Pleistocene and Holocene. *Earth's Cryosphere* XXVIII (3), 3–16.

Approaching the truth  
is the sum of many opinions.

*Yulian Semenov*

## INTRODUCTION

The modern geologic and geomorphologic patterns of the north of the West Siberian Plate were formed in the Quaternary period under the influence of a complex of geological processes. In the sedimentary cover, there are indicators of both aggradation and degradation of permafrost and neotectonic movements: features attesting to sediment freezing and thawing, decomposition of gas hydrates, cryogenic formations, folded and fault deformations, etc. [Andreev, 1960; Trofimov et al., 1987; Badu, 2011].

There are different concepts about the geological and climatic events that occurred in the north of Western Siberia during this period [Arkhipov et al., 1994; Sidorchuk et al., 2008; Astakhov, 2009]. Paleogeographic reconstructions are not always sufficiently proved by the facts and do not always consider the influence of cryolithogenesis. Thus, the origin of the hollow-ridge landforms in Western Siberia is associated with neotectonic uplifts and subsidences controlled by meridional and latitudinal fault systems [Gorodetskaya, 1972], transgressions and regressions of the sea, the

formation of a series of terraces due to eustatic fluctuations in the level of the Polar Basin [Kuzin, 2005; Savchenko, 2016], as well as with the activity of land and shelf glaciers [Grosswald, 1983; Astakhov, 2009; Nazarov, 2015]. Less often, they are associated with the erosive activity of rivers and permafrost thawing [Sidorchuk et al., 2008] or with cryoarid desertification [Zykina et al., 2017; Pozdnyakov et al., 2020].

P.E. Bragin [2001] noted that the Pliocene–Quaternary negative structures within the West Siberian Plate are often attributed to erosional downcutting regardless of their geological structure, while completely denying the possibility of neotectonic movements. Data on the distribution of “folds and ruptures of gravitational slumps” formed during the renewal of basement faults in the Late Cenozoic and Quaternary appeared later [Gusev, 2015]. E.A. Manuilova [2021] associated the activation of erosion and erosion-denudation processes and, as a consequence, the formation of swampy and lake depressions in fault zones with neotectonic uplifts.

The most difficult task is to determine the time of action of neotectonic and erosional processes and the impact of freezing-thawing of sediments. To clarify the age of geological events, radiocarbon dating of sections, permafrost facies analysis, determination of cryogenic origin, and identification of deformations of terrigenous sediments are used [Slagoda, Medvedev, 2004; Kaplina, 2009; Katasonov, 2009; Tumskoy, 2021]. Neotectonic movements in a structure of the sedimentary sequence are identified on the basis of changes in the hypsometric position of a roof of coeval layers, deformations of bedding, cryogenic and paleocryogenic formations [Slagoda et al., 2001, 2015].

### STUDY AREA AND RESEARCH METHODS

The studied area is located in the northeastern part of the Pur–Taz interfluvium (Fig. 1A). In terms of tectonic structure, this is the north of the Urengoy and Khudoseya megatroughs [Ershov, 1989]. According to the *Structural Geomorphologic Map of the West Siberian Plate* [Manuilova, 2021], the study area is located within the Taz depression of the Nadym–Taz neotectonic region. The relief of the depression is gently hilly, with local uplifts (ridges) with flat tops and gentle slopes, isometric and elongated shape, and the northeastern and meridional strike. The drainage pattern includes the Taz River, valleys of small rivers, and thermokarst-erosion hollows, which are confined to a diagonal network of faults and fractures [Filipovich, 2012].

The valley complex of modern low terraces of the Taz River and the third Late Pleistocene polygenetic (lacustrine-alluvial) terrace (plain) are distinguished in the geomorphologic structure of the area [Melnikov, Moskalenko, 1991]. The plain includes elevated ridges and thermokarst-erosional hollows with khasyreys (alases). Ridges are elevated at about 20–50 m a.s.l. and act as divides for small rivers with the water level of 1.6–8.8 m a.s.l. Relict polygonal landforms complicate the surface of ridges. Thermokarst depressions with lakes (khasyreys) are located at different levels: from 5.3 to 17.4 m a.s.l. (Fig. 1B). Polygonal peatlands with ice wedges, the formation of which began 12–9 ka BP, are attributed to the khasyreys. Most of the peat was accumulated during the first half of the Holocene and in the Holocene optimum [Trofimov et al., 1987; Vasil'chuk, Vasil'chuk, 2016]. The sediments underlying peat have not been dated previously.

The study area is located in the zone of continuous ice-bonded permafrost of 200–350 m in thickness [Ershov, 1989]. Rock temperature at a depth of zero annual temperature amplitudes (7–15 m) is –2.7 to –2.4°C on sandy-loamy ridges, and –4 to –2°C in peat khasyreys. The depth of seasonal thawing on sandy ridges varies from 1.05 to 2.4 m; in depressions with peat, from 0.35 to 0.65 m [Khomutov et al., 2019; Babkina et al., 2022].

To analyze the geocryological structure and to correlate and reconstruct the environmental changes in the Late Pleistocene and Holocene, we used sections from three boreholes and five pits described and sampled in 2016–2021 within the framework of comprehensive studies of the Pur–Taz interfluvium. The data on these studies were partially published in the articles devoted to other issues of geocryology (Table 1). The authors determined the composition and cryogenic structure of sediments in the sections and collected samples to analyze particle-size distribution and to identify the species composition and age of plant remains. Particle-size distribution analysis of sediments (102 samples) was performed in the Cryotraceology Laboratory of the Institute of Earth Cryosphere, Tumen Scientific Center, Siberian Branch of the Russian Academy of Sciences on the Mastersizer 3000 laser diffraction particle-size analyzer by E.S. Koroleva. The distribution of particle size s determined in the samples on the R. Passega dynamic diagram [Reinek, Singh, 1975] and their sedimentary layering were used to clarify the environments of sediment accumulation. The species composition of plant remains (23 samples) was determined at the Institute of Earth Cryosphere, Tyumen Scientific Center, Siberian Branch of the Russian Academy of Sciences by A.O. Kuznetsova using the microscopic method based on atlases-determinative guides and a collection of microslides of modern tundra plants.

Radiocarbon dating of the samples of plant remains with IGAN<sub>AMS</sub> index (14 samples) was carried out in the Collective Use Center Laboratory of Radiocarbon Dating and Electron Microscopy at the Institute of Geography, Russian Academy of Sciences (Moscow) and in the Center for Isotope Studies of the University of Georgia (USA). Radiocarbon age of samples with the IMCES index (39 samples) was determined by the liquid scintillation method on the Quantulus spectrometer-radiometer of the Tomsk Regional Collective Use Center, Tomsk Scientific Center, Siberian Branch, Russian Academy of Sciences. Data calibration was performed in the CALIB

### Fig. 1. Study area (A) and location of boreholes and cuts on the III lacustrine-alluvial plain (B).

1 – low terrace of the Taz River; 2–7 – III lacustrine-alluvial plain (2 – valleys of small rivers; 3 – relief depressions, hollows below 20 m a.s.l.); 4 – khasyreys; 5–7 – uplands with heights of 5 – 40–50 m, 6 – 30–40 m, and 7 – 20–30 m a.s.l.; 8 – hydrosystem (lakes and streams); 9 – surface height, m a.s.l.; 10 – mining excavations: (a) boreholes, (b) cuts and exposures; 11 – (a) roads, (b) settlements.

FORMATION OF THE HOLLOW-RIDGE TOPOGRAPHY ON THE PUR-TAZ INTERFLUVE

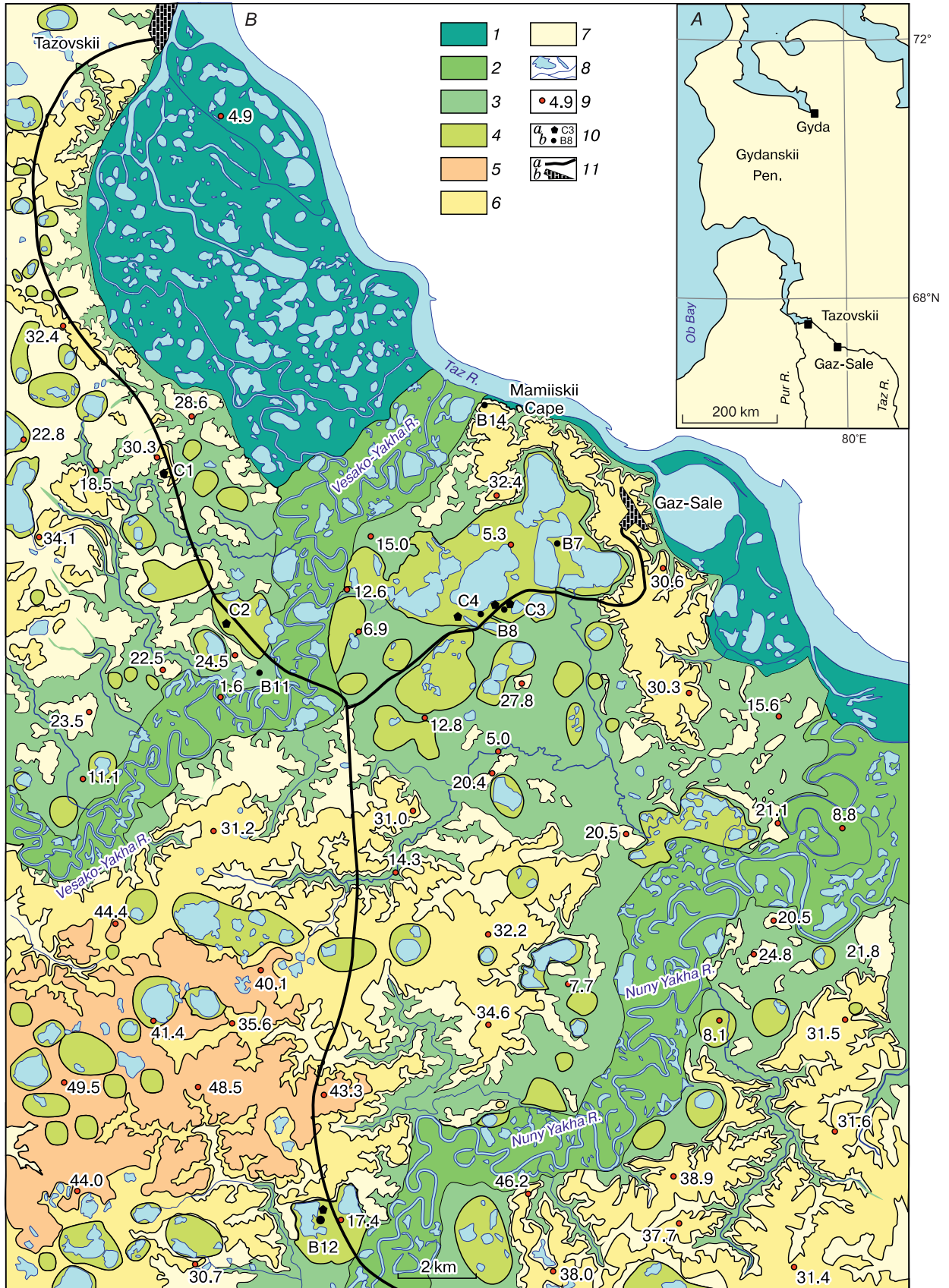


Table 1. Mining excavations in the study area

| Position in relief | Type* and number | Abs. height of the surface, m a.s.l. | Depth, m |
|--------------------|------------------|--------------------------------------|----------|
| Ridge              | C1               | 28                                   | 9        |
|                    | B11              | 12                                   | 2.0      |
|                    | B14              | 31                                   | 1.5      |
| Hollow             | C3               | 8                                    | 13       |
|                    | C4               | 8                                    | 7        |
|                    | B7               | 10–11                                | 4        |
|                    | B8               | 7–8                                  | 2.2–2.4  |
|                    | B12              | 17                                   | 2.2      |

\* C – borehole, B – pit or exposure.

REV8.2 program [Stuiver, Reimer, 1993; Hua et al., 2013]. Calibration curves and age calculation methods are updated very often; therefore, following N.A. Khotinsky [1977] and A.A. Velichko [Velichko et al., 2017], we present radiocarbon dates in the uncalibrated (before present (1950), years BP) [Zazovskaya, 2016] and calibrated (years cal BP) format (Table 2) for comparison with paleoclimatic subdivisions [Zhamoyda, 2019]. The sections were correlated by comparing the lithological composition, structure, age of sediments, and paleocryogenic features; layers were numbered from bottom to top along the most complete section of borehole C1.

### CHARACTERISTICS OF THE SECTIONS

The structure of the upper part of the ridges of the third lacustrine-alluvial plain was studied in borehole C1 and exposures B14 and B11 (Fig. 1). Core samples from the borehole represented the Lower Karginsk channel and floodplain sediments (layers 1–3), undated lacustrine sediments (layer 4), and presumably Sartan slope sediments (layer 5); all of them display postcryogenic structures. Layers 3 and 5 include ice-wedge casts. A detailed description of the borehole section is given in [Slagoda et al., 2022].

On the ridge, in the pit studied on Mamii Cape (B14), loams with cryoturbation and humified loamy sands occur under the surface layer. These sediments

fill subsidences above ground wedges (layer 5, Fig. 2A). The wedges have vertical dimensions of more than 1.5 m and the width of 0.5–1.0 m at the top; their axes are inclined down the slope. Lower parts of ground wedges have not been completely uncovered. At the edges, the wedges are filled by horizontally layered sand broken by fractures into small blocks; in the center, sand is fine-grained, contains ocherous mottles and displays vertical wavy bedding. The host sands are slightly displaced along diagonal subsidence cracks, and their bedding is complicated by postcryogenic textures with ferrugination.

The morphology of sediments in the lower part of the ridge was studied in the exposed wall of a quarry (Fig. 2B, B11). Under technogenic surface soil with inclusions of peat (layer 9) dated to 1954 (Table 2), a frozen stratum composed of deformed layered sands and loamy sands with postcryogenic platy structure (layers 3, 4) was described. This stratum contains wedge-shaped structures of 0.8–1.5 m in height 0.7–1.2 m in width at the top. The wedges are composed of ferruginated loams, loamy sands, and sands with vertical wavy bedding; their vertical axes are inclined and displaced downslope. At the contacts with the ground wedges, the bedding of the host sands and loamy sands is curved upward, and their blocks are displaced along settling cracks (Fig. 2B). Fragments of the polygonal network were uncovered higher up the slope.

The structure of the thermokarst-erosional hollow was studied in khasyreys with polygonal palsa (flat-topped frozen peat mounds) peatlands on the basis of core samples from boreholes C3 and C4 and exposures B7, B8, and B12 (Fig. 3).

The structure of the polygonal peatland was studied in exposure B7 at a distance of 0.5 km from the ridge. The upper peat layer of 1.0–1.5 m in thickness and the age of 9200–5700 BP is dissected by an ice wedge of more than 1.5 m in height (layer 7). The peat overlies lacustrine loamy sand with a lens-type cryostructure (layer 6) and tabular sediments – sands and loamy sands with decomposed organic matter, crumpled layering, ferrugination, and massive and

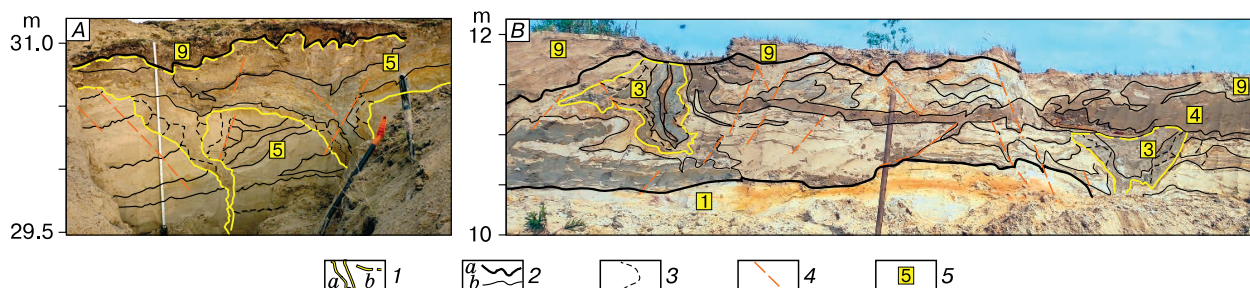


Fig. 2. Ground wedge structures in sections of the ridge, exposures B14 (A) and B11 (quarry) (B).

1 – outlines of pseudomorphs (a) proved, (b) assumed; 2 – (a) layer boundaries, (b) layering; 3 – subsidence blocks; 4 – fragments of fractures of displacement; 5 – layer numbers.

## FORMATION OF THE HOLLOW-RIDGE TOPOGRAPHY ON THE PUR-TAZ INTERFLUVE

Table 2. Results of radiocarbon dating of peat

| No.                                      | Index                     | Layer | Depth, m  | Composition                                 | Radiocarbon age, ( $1\sigma^*$ ), yr | Calibrated age, yr BP |
|--|---------------------------|-------|-----------|---|--------------------------------------|-----------------------|
| 1  | 2                         | 3     | 4         | 5   | 6                                    | 7                     |
| <b>Borehole C1, polygon</b>              |                           |       |           |   |                                      |                       |
| 1  | IGAN <sub>AMS</sub> -5827 | 1     | 5.2–5.4   | Plant remains, washed–in moss, detritus     | 45 205 ± 400                         | 48 058–49 179         |
| 2  | IGAN <sub>AMS</sub> -5828 | 1     | 7.6–7.7   | Plant remains, washed–in moss, detritus     | 49 110 ± 610                         | 51 212–52 740         |
| <b>Borehole C3, polygon</b>              |                           |       |           |   |                                      |                       |
| 3  | IMCES-14C2047             | 7     | 0.6–0.7   | Peat autochthonous                          | 5653 ± 130                           | 6303–6562             |
| 4  | IGAN <sub>AMS</sub> -8613 | 7     | 2.5–2.55  | Peat autochthonous                          | 6130 ± 20                            | 6953–7010             |
| 5  | IMCES-14C2051             | 7     | 2.8–2.89  | Peat autochthonous                          | 7495 ± 140                           | 8170–8420             |
| 6  | IGAN <sub>AMS</sub> -8614 | 7     | 2.8–2.89  | Peat autochthonous                          | 7010 ± 25                            | 7831–8650             |
| 7  | IGAN <sub>AMS</sub> -8615 | 6     | 3.9–4.0   | Peat autochthonous                          | 8040 ± 25                            | 8981–9010             |
| 8  | IGAN <sub>AMS</sub> -8616 | 6     | 4.2–4.3   | Peat autochthonous                          | 10 165 ± 30                          | 11 804–11 879         |
| 9  | IGAN <sub>AMS</sub> -8618 | 6     | 4.6–4.65  | Plant remains washed–in, grass roots        | 10 900 ± 30                          | 12 766–12 824         |
| 10                                       | IGAN <sub>AMS</sub> -8619 | 4     | 5.5–5.9   | Plant remains, washed–in branches, detritus | 21 490 ± 50                          | 25 779–25 882         |
| 11                                       | IGAN <sub>AMS</sub> -8620 | 4     | 8.0–8.2   | Plant remains, washed–in branches, detritus | 21 290 ± 50                          | 25 636–25 757         |
| 12                                       | IGAN <sub>AMS</sub> -8621 | 4     | 8.3–8.4   | Plant remains, washed–in branches, detritus | 19 105 ± 45                          | 22 963–23 045         |
| 13                                       | IGAN <sub>AMS</sub> -8622 | 4     | 8.4–8.45  | Plant remains, washed–in branches, detritus | 17 860 ± 40                          | 21 479–21 594         |
| 14                                       | IMCES-14C2040             | 4     | 8.3–9.0   | Plant remains, washed–in branches, detritus | 20 148 ± 350                         | 22 704–21 863         |
| 15                                       | IGAN <sub>AMS</sub> -8623 | 1     | 12.1–12.2 | Plant remains, washed–in branches, detritus | >49 755                              |                       |
| <b>Borehole C4, polygon</b>              |                           |       |           |   |                                      |                       |
| 16                                       | IMCES-14C2056             | 8     | 0.7–0.78  | Peat autochthonous                          | 3313 ± 120                           | 3440–3650             |
| 17                                       | IMCES-14C2063             | 7     | 2.3–2.4   | Peat autochthonous                          | 7111 ± 160                           | 7743–8038             |
| 18                                       | IMCES-14C2068             | 6     | 3.5–3.6   | Peat autochthonous                          | 8740 ± 145                           | 9544–9909             |
| <b>Pit B8, interpolygonal depression</b> |                           |       |           |   |                                      |                       |
| 19                                       | IMCES-14C1488             | 9     | 0–0.07    | Vegetation cover, peat                      | 897 ± 90                             | 730–834               |
| 20                                       | IMCES-14C1487             | 8     | 0.07–0.12 | Peat autochthonous                          | 2766 ± 78                            | 2779–2939             |
| 21                                       | IMCES-14C1459             | 7     | 0.12–0.2  | Peat autochthonous reddish brown            | 5417 ± 114                           | 6169–6304             |
| 22                                       | IMCES-14C1486             | 7     | 0.2–0.26  | Peat autochthonous reddish brown            | 5670 ± 83                            | 6392–6555             |
| 23                                       | IMCES-14C1456             | 7     | 0.26–0.34 | Peat autochthonous dark brown               | 5953 ± 95                            | 6667–6896             |
| 24                                       | IMCES-14C1470             | 7     | 0.34–0.4  | Peat autochthonous reddish                  | 5968 ± 96                            | 6673–6901             |
| 25                                       | IMCES-14C1462             | 7     | 0.8–0.9   | Peat autochthonous black                    | 7766 ± 75                            | 8446–8599             |
| 26                                       | IMCES-14C1473             | 6     | 1.4–1.5   | Peat autochthonous reddish, layered         | 8039 ± 101                           | 8722–9026             |
| 27                                       | IMCES-14C1454             | 6     | 2.2–2.3   | Roots, branches autochthonous               | 8410 ± 82                            | 9403–9527             |
| 28                                       | IMCES-14C1477             | 6     | 2.2–2.3   | Peat autochthonous from moss, brown         | 8413 ± 91                            | 9401–9530             |
| <b>Pit B7, polygon</b>                   |                           |       |           |   |                                      |                       |
| 29                                       | IMCES-14C1512             | 9     | 0–0.07    | Soil with roots, thawed                     | 134 ± 70                             | <b>1660–1960 AD**</b> |
| 30                                       | IMCES-14C1513             | 7     | 0.07–0.23 | Peat autochthonous black, brown             | 5688 ± 120                           | 6392–6572             |
| 31                                       | IMCES-14C1483             | 6     | 0.23–0.4  | Peat autochthonous reddish, loose           | 8247 ± 82                            | 9122–9310             |
| 32                                       | IMCES-14C1472             | 6     | 0.4–0.45  | Peat autochthonous brown                    | 8382 ± 102                           | 9282–9493             |
| 33                                       | IMCES-14C1482             | 6     | 0.45–0.47 | Peat autochthonous black                    | 8596 ± 82                            | 9523–9668             |
| 34                                       | IMCES-14C1474             | 6     | 0.47–0.55 | Peat with branches, birchbark, brown        | 8718 ± 94                            | 9547–9785             |
| 35                                       | IMCES-14C1464             | 6     | 0.55–0.72 | Peat autochthonous from grass, moss, brown  | 8648 ± 108                           | 9529–9773             |
| 36                                       | IMCES-14C1469             | 6     | 0.72–0.89 | Peat autochthonous reddish                  | 9117 ± 91                            | 10 200–10 405         |
| 37                                       | IMCES-14C1468             | 6     | 0.72–0.88 | Twigs, roots, autochthonous                 | 9226 ± 102                           | 10 257–10 445         |
| <b>Pit B8, polygon</b>                   |                           |       |           |   |                                      |                       |
| 38                                       | IMCES-14C2073             | 9     | 0.05–0.25 | Peat autochthonous from moss, thawed        | 1627 ± 65                            | 1408–1548             |
| 39                                       | IMCES-14C2069             | 8     | 0.3–0.48  | Peat autochthonous, thawed, dense           | 4027 ± 165                           | 4349–4657             |
| 40                                       | IMCES-14C2060             | 7     | 0.5–0.7   | Peat autochthonous from moss, frozen        | 5662 ± 120                           | 6309–6560             |
| 41                                       | IMCES-14C2067             | 7     | 0.75–0.8  | Peat autochthonous from moss                | 6050 ± 95                            | 6782–7005             |
| 42                                       | IMCES-14C2072             | 7     | 1.0–1.1   | Peat autochthonous from moss, grass, twigs  | 6245 ± 85                            | 7154–7257             |
| 43                                       | IMCES-14C2054             | 7     | 1.3–1.4   | Peat autochthonous from moss, grass, twigs  | 6323 ± 110                           | 7157–7357             |

| 1   | 2                        | 3 | 4        | 5   | 6            | 7                |
|---|--------------------------|---|----------|---|--------------|------------------|
| 44  | IMCES-14C2066            | 7 | 1.6–1.7  | Peat autochthonous from moss, grass, twigs  | 6730 ± 105   | 7505–7677        |
| 45  | IMCES-14C2058            | 7 | 1.9–2.0  | Peat autochthonous from moss, grass, twigs  | 6920 ± 125   | 7662–7866        |
| <b>Exposure B11, quarry, technogenic formations</b> |                          |   |          |   |              |                  |
| 46  | IGAN <sub>AMS</sub> 8624 | 1 | 5.0–5.5  | Plant remains, detritus of moss             | 1.03 ± 0.003 | <b>1954 AD**</b> |
| <b>Cut B12, polygon</b>                             |                          |   |          |   |              |                  |
| 47  | IMCES-14C2059            | 7 | 0.2      | Peat autochthonous, thawed                  | 7227 ± 100   | 7962–8056        |
| 48  | IMCES-14C2053            | 6 | 0.55–0.6 | Peat autochthonous from moss, grass, frozen | 8264 ± 120   | 9122–9331        |
| 49  | IMCES-14C2055            | 6 | 0.6–0.65 | Peat autochthonous from moss, grass, twigs  | 8598 ± 120   | 9468–9747        |
| 50  | IMCES-14C2062            | 6 | 0.65–0.7 | Peat autochthonous from moss, grass, twigs  | 8130 ± 155   | 8971–9295        |
| 51  | IMCES-14C2046            | 6 | 1.15–1.2 | Peat autochthonous from moss, grass, twigs  | 8519 ± 130   | 9406–9675        |
| 52  | IMCES-14C2107            | 6 | 1.5–1.65 | Peat autochthonous from moss, grass, twigs  | 8730 ± 130   | 9543–9905        |
| 53  | IMCES-14C2044            | 6 | 2.0–2.1  | Peat autochthonous from moss, grass, twigs  | 8576 ± 175   | 9415–9818        |

Note: IMCES – Institute of Monitoring of Climatic and Ecological Systems.

\* 1σ – probability 68%.

\*\*AD calendar years.

lens-type cryostructures [Slagoda et al., 2019]. The lower part of the peat layer is composed of mosses (*Sphagnum magellanicum* Brid and hypnum mosses), sedges, and dwarf birch remains. In the middle part of the peat layer, the content of sedges (*Carex rotundata* and *C. pauciflora* Lightf.) increases; the remains of burnet (*Sanguisorba tenuifolia* Fisch.), horsetail (*Equisetum palustre* L.), and sphagnum mosses are also present. The upper peat layer mainly consists of sphagnum mosses; hypnum mosses (*Drepanocladus aduncus* (Hedw.)), liverwort mosses, and rush (*Juncus filiformis* L.) are present [Kuznetsova et al., 2022].

The structure of the polygonal peatland at a distance of 4–5 km from the ridge was studied in core samples from boreholes C3 and C4 and in exposure B8. The peat is dissected by ice wedges with visible vertical dimensions of 1.5–2.2 m and the width at the top of about 0.8–2.2 m [Tikhonravova et al., 2020; Koroleva, 2022].

Borehole C3 was laid in the center of the polygon. In the lower part (layer 1, Fig. 3), the core sample consists of sands with crushed coal, graphite, amber, and allochthonous remains of dwarf shrubs and mosses; with massive and thin lens-type cryostructures. The sand displays cross-bedding with thin layers slipping along closed fractures by 1–5 cm. Layer 1 is dated to the beginning of the Karginsk thermochron, more than 50 ka BP (Table 2). No analogues of layer 2 discovered on the ridge (borehole C1, exposure B11) were identified in borehole C3. Layer 3 overlying layer 1 is represented by nonlayered sand with crumb structure and with a tongue of loamy sand penetrating to a depth of 2 m from the top, whose origin was probably caused by subsidence of sediments (Fig. 4). The top of layer 3 is eroded and is overlain by cross-bedded sands with the washed-in organic matter (layer 4). Above it, there are sands

with the washed-in plant remains and horizontal layering (layer 5). The age of the layer is 21 500–17 800 BP, the first half of the Sartan Cryochron (Table 2). At the depths of 5.5–10.5 m, inversion is manifested in the distribution of dates: the lower dates are younger, the upper ones are older. Silty sands with interlayers of loamy sand and washed-in plant detritus (layer 6) overlie the eroded surface of layer 5. These sands accumulated in 10.9–8 ka BP (Fig. 3, Table 2). They are overlain by autochthonous 4.2-m-thick peat (layer 7). From a depth of 0.4 m, the peat is frozen and displays diverse (massive, lens-type, and banded) cryostructures (Fig. 4). Sedges (*Carex vesicaria*), hypnum mosses, remnants of horsetail and birch, and, less frequently, crowberry (*Empetrum nigrum*) predominate in the lower part of the peat layer. The middle part is characterized by an increase in the share of hypnum mosses, dwarf shrubs (*Betula nana*, *Empetrum nigrum*), and herbs (*Eriophorum russeolum*, *Calla palustris*, *Carex inflata*, *Equisetum arvense*). The upper part consists of the remains of sedges (*Carex vesicaria*), horsetail, less often ringless-hook moss (*Warnstorfia exannulata*), dwarf birch (*Betula nana*), and ledum (*Ledum decumbens*) [Kuznetsova et al., 2022]. The peatland formation lasted from 8 to 5.7 ka BP.

Borehole C4 uncovered similar silty sands and loamy sands with interlayers of the washed-in organic matter in the form of fine detritus, plant roots, and branch fragments (layers 4, 5); loamy sand (layer 6); and the upper peat layers (layers 7, 8, 9) with a total thickness of 3.6 m. Sediments are frozen from a depth of 0.4 m; reticulate, lens-type, and massive cryostructures predominate. The peat layer was formed in the interval from 9900 to 3400 BP.

The peat layer in the interpolygonal depression above the ice wedge was studied in pit B8 to a depth

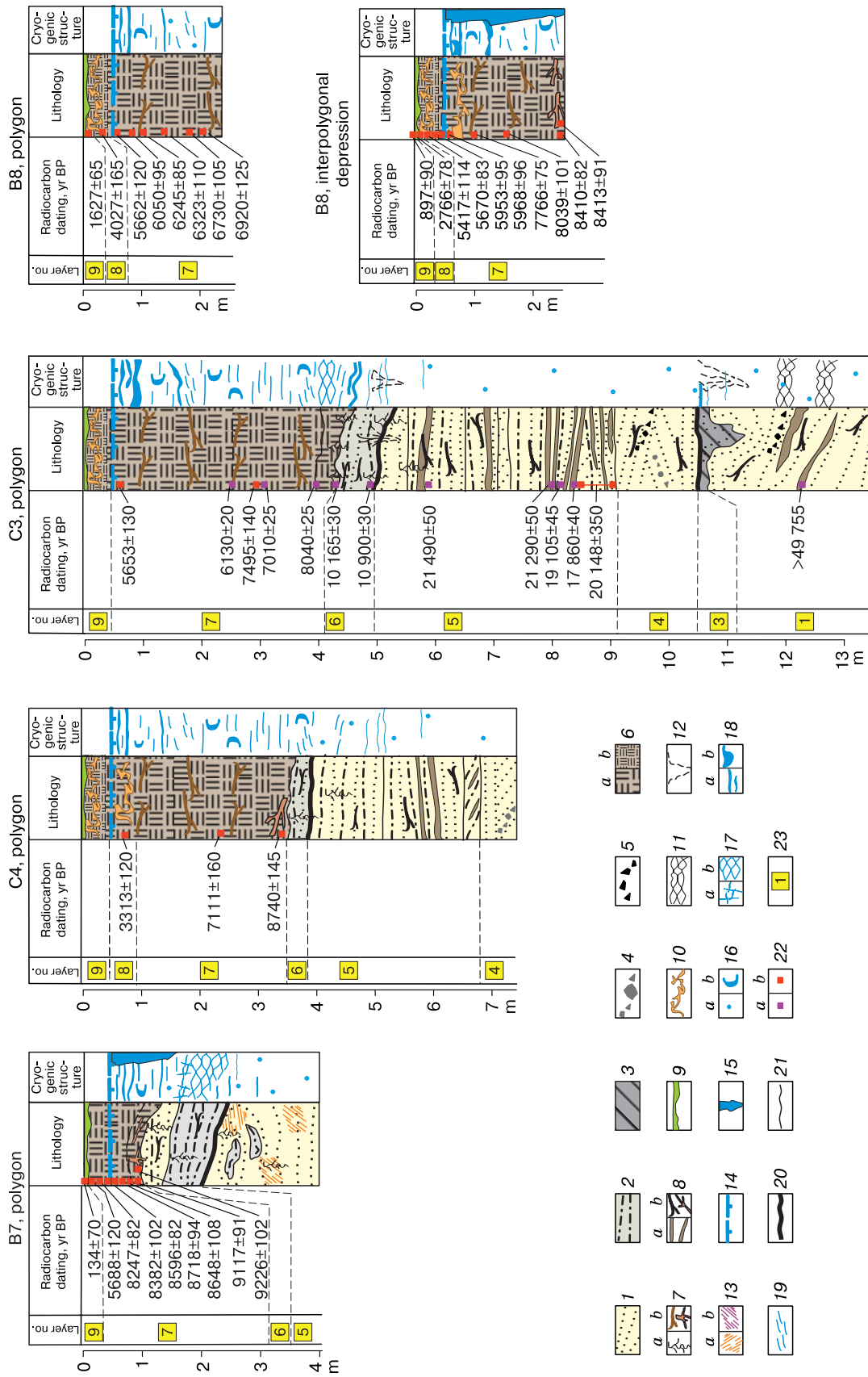


**Fig. 3. Cryolithological structure of khasyrey deposits of the lacustrine-alluvial plain of the Pur-Taz interfluvium.**

1 – layered sand; 2 – loamy sand; 3 – loam; 4 – interlayers of mudstone grass and clay galls; 5 – charcoal, charred wood; 6 – autochthonous (a) loose peat, (b) dense peat; 7 – roots, branches, *in situ* stems of (a) grasses, (b) dwarf shrubs, trees; 8 – washed-in (a) detritus, (b) rounded branches, chips; 9 – soil, moss with roots of modern plants; 10 – cryoturbations; 11 – postcryogenic structures; 12 – tongues, subsidences; 13 – mottles, streaks of (a) ferric, (b) ferrous compounds; 14 – permafrost table; 15 – ice wedges. Cryogenic structures: 16 – (a) massive, (b) crusted; 17 – (a) cellular reticulated, (b) incompletely lattice; 18 – (a) banded, (b) with large ice inclusions; 19 – lens-type, Boundaries: 20 – erosional; 21 – lithological; 22 – samples for radiocarbon age determination in the (a) Institute of Geography, Russian Academy of Sciences (IGAN<sub>AMS</sub>) and (b) Institute of Monitoring of Climatic and Ecological Systems, Siberian Branch of the Russian Academy of Sciences; 23 – layer number. The present time is 1950.

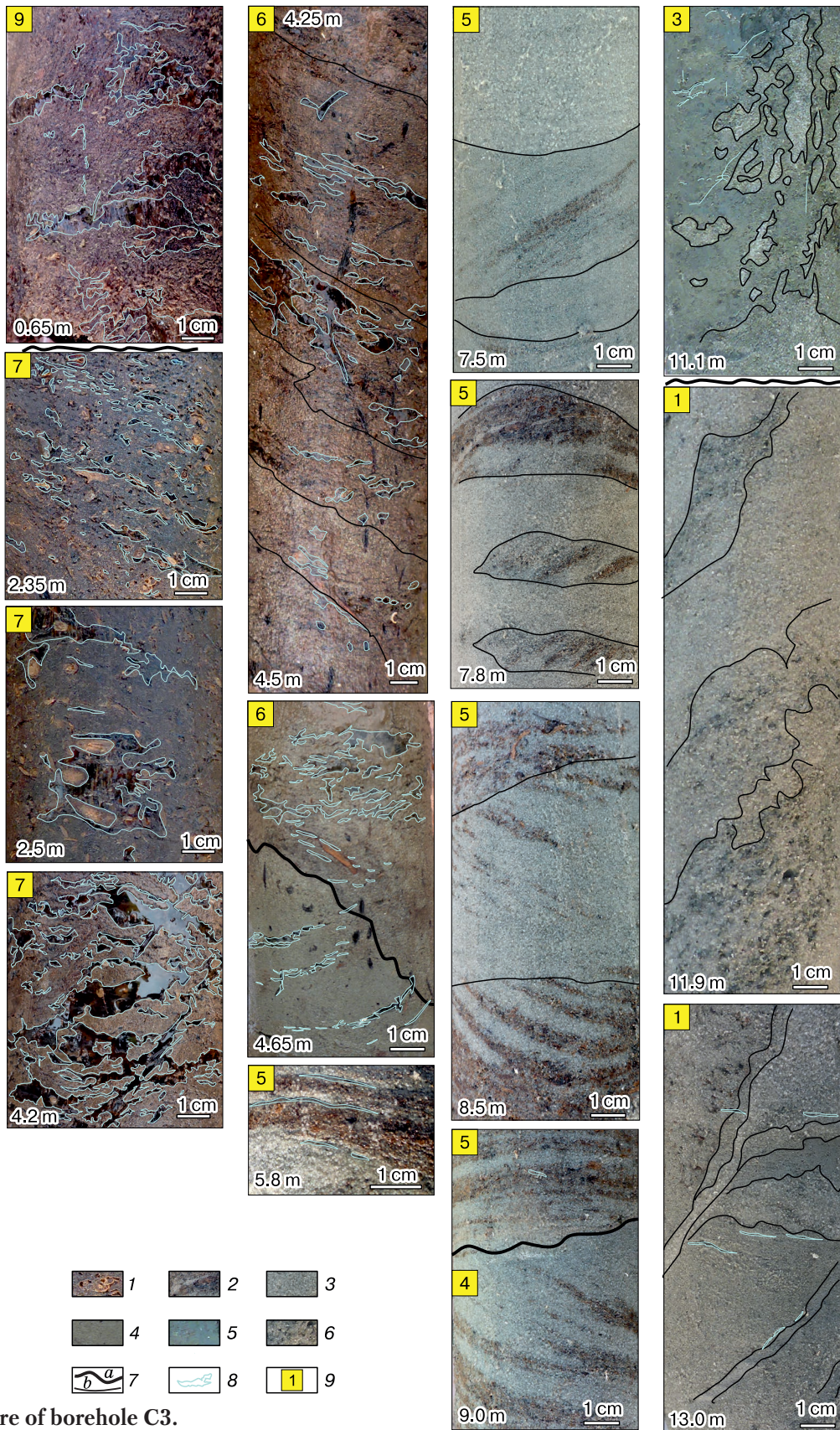


**Fig. 4. Core of borehole C3.**

1 – autochthonous peat; 2 – washed-in plant remains; 3 – medium- and fine-grained sand; 4 – silty sand; 5 – loam; 6 – sand with washed-in particles of mudstone, charcoals, charred wood, clay rocks; 7 – lithological boundaries; 8 – outlines of ice inclusions; 9 – layer number.

of 2.4 m. From a depth of 0.5 m, the peat was frozen, with massive, banded, and crust-type cryostructures [Tikhonravova et al., 2020]. In the lower part, the peat consists of the remains of willows (*Salix* sp.), horsetails (*Equisetum palustre*), sedges (*Carex rotundata*), and dwarf shrubs (*Vaccinium uliginosum*). In the middle part, it mainly consists of sedges (*Carex rotundata*, *Eriophorum medium*, *Carex globularis*); the remains of dwarf birch, sphagnum, and hypnum mosses are present; and the content of horsetail remains decreases. The upper part of the peat layer is composed of sphagnum mosses (*Sphagnum magellanicum*, *Sph. balticum*, *Sph. angustifolium*, *Sph. wanstorffii*); cinquefoil (*Comarum palustre*), cotton grass (*Eriophorum medium*), and dwarf shrubs (*Vaccinium vitis-idaea*, *Ledum palustre*) are present; the content of horsetail and dwarf birch remains decreases [Kuznetsova et al., 2022]. The accumulation of the studied part of the peat took place from 8400 to 5400 BP. Autochthonous peat (layer 7) was uncovered in the khasyrey polygon by pit B12. It was frozen from a depth of 0.75 m, with a predominance of crust-type, lens-type, and banded cryostructures [Koroleva, 2022]. The accumulation of the uncovered peat layer occurred in 8700–7200 BP.

The studied sediment sections on the ridge differ from those in the hollow by their cryogenic structure, the set of identified layers, and the absence of a thick peat upper peat layer. Layers 1–6 were compared with respect to their bedding typical of permanent and temporary watercourses with variable intensity of the flow and the distribution of characteristic grain-size points on the R. Passega dynamic diagram [Reinek, Singh, 1975] (Fig. 5). According to the sequence of the layers, the presence of pseudomorphs by ice wedges, postcryogenic features, and radiocarbon age, seven layers were identified in the sections studied on the ridge: Karginsk–Sartan (layers 1–5) and, presumably, Sartan–Holocene (layers 6 and 9); the sections studied in the hollow were somewhat different: Karginsk–Sartan (layers 1–6, but without layer 2) and Holocene (layers 7–9).

#### Correlation of the sections of the upper part of permafrost on the ridges and in the hollow

The integrated section of the III lacustrine-alluvial plain was compiled on the basis of correlation of the sections studied on the ridges and in the hollow (Fig. 6). The Lower Karginsk sediments (49–45 ka BP, layers 1–3, boreholes C1, C3) were identified on the ridges and in the hollow (under the khasyreys).

Layer 1 – cross-bedded sands with charred wood and moss; according to their position on the Passega diagram, they accumulated in a permanent watercourse with varying intensity of the flow; these sediments were attributed to the channel alluvium.

Layer 2 – loamy sand and sand with washed-in remains of shrubs and mosses; these sediments accu-

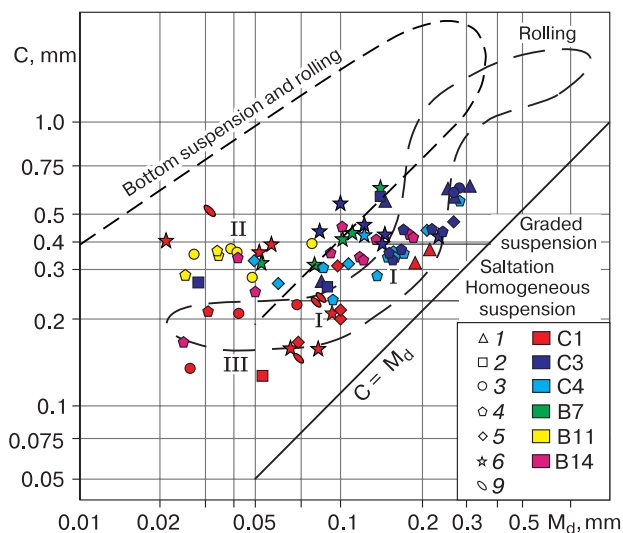


**Fig. 5. Dynamic diagram of R. Passega – lithologic types of sediments of lacustrine-alluvial terrace III.**

Sedimentation settings (I–III): I – sediments of active and weakly dynamic permanent watercourses; II – sediments of temporary watercourses, proluvium, deluvium (colluvium); III – sediments of flow-through shallow water bodies.  $M_d$  – median diameter (particle diameter, relative to which 50% of the sample particles have smaller (and larger) diameter);  $C$  – maximum diameter (99% of particles have smaller diameter). Geometric figures: figure number corresponds to the layer number; figure color corresponds to the name of the section (exposure).

mulated in a permanent watercourse with low or moderate intensity of the flow and were attributed to the floodplain facies of the alluvium (Fig. 5). These sediments were presumably formed because of the erosion of the Jurassic coaly sandstones with graphite and amber, Paleogene mudstones, or Pleistocene marine clays [Decision..., 2004].

Layer 3 on the ridge is represented by layered sandy loams and sands with ground wedges; the lack of distinct bedding and the fine-grained texture suggest sedimentation in shallow flowing lakes [Slagoda et al., 2022]. The shape of ground wedges (B11, B14, Fig. 2), their relatively large size, the presence of settling and sliding blocks along the lateral contacts, and vertical wavy bedding in the wedges, as well as the bends in the layers of host sediment suggest that the wedges described in the section of borehole C1 represented pseudomorphs that substituted initial ice wedges. In the hollow, layer 3 is composed of sands with washed-in vegetation debris and inclined bedding. Taking into account the position of these sands on the Passega diagram (Fig. 5), it can be supposed that their accumulation took place in a permanent watercourse with moderate to low intensity of the flow. A large (more than 1 m) vertically oriented tongue of loamy sands and sands (C3, Fig. 4) in layer

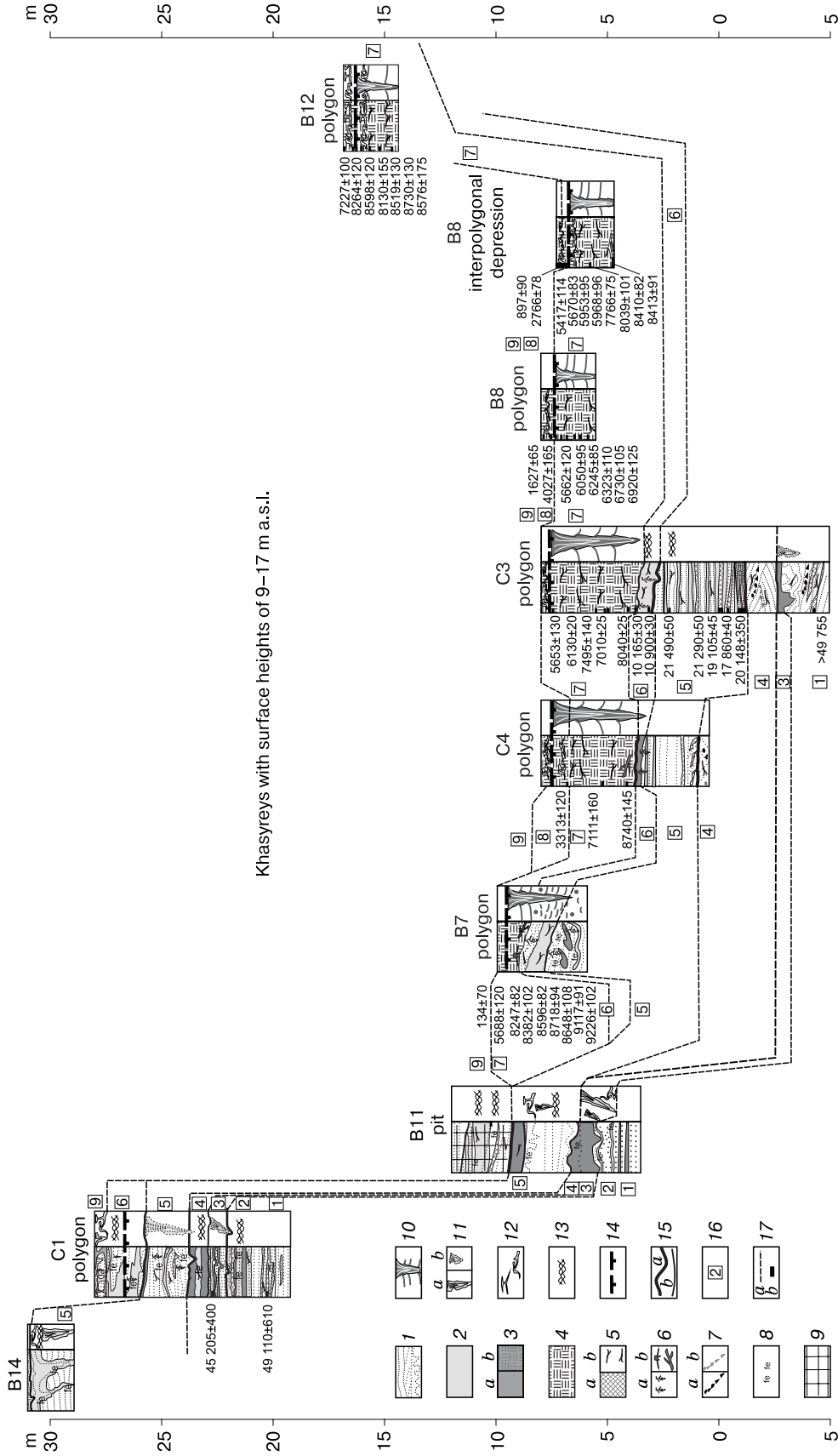


**Fig. 6. Correlation of sediments of watersheds and khasyres of III lacustrine-alluvial terrace of the Pur–Iaz interfluvium.**

1 – layered sand; 2 – loamy sand; 3 – (a) loam and clay, (b) peaty loam; 4 – autochthonous peat; 5 – (a) allochthonous peat, (b) plant detritus, twigs; 6 – (a) thread-like roots of herbs *in situ*, (b) stumps, trunks *in situ*; 7 – (a) charcoal inclusions, admixtures of graphite, amber, (b) mudstones; 8 – ocherous iron compounds; 9 – technogenic-displaced sediments; 10 – ice wedges; 11 – pseudomorphs in place of ice wedges; (a) reliable in cuts and exposures; (b) assumed from borehole cores; 12 – cryoturbations, cryogenic involutions; 13 – postcryogenic structures; 14 – upper boundary of frozen rocks; 15 – (a) erosional and (b) lithologic boundaries; 16 – layer number; 17 – radiocarbon dating.

3 is also attributed to a pseudomorph based on its similarity to the structure of the wedge in the section of borehole C1. The age of the pseudomorph is less than the age of the Lower Karginisk host sediments, because the growth of ice wedges could take place simultaneously or after the accumulation of lacustrine-alluvial sediments, and their melting surely occurred later. The top of the Lower Karginisk deposits is partially eroded and located at different hypsometric levels of plain III: at 23–10 m a.s.l. on the ridges and 4 m below sea level within the thermokarst-erosional hollow; thus, the amplitude of heights reaches 14–27 m.

Layer 4 in section on the ridge is composed of loams and loamy sands with washed-in plant remains and vivianite; presumably, it is of Karginisk age. According to characteristic features of horizontal layering and the position of the layers on the Passega diagram (from the region of homogenous bottom suspensions to various grades of suspensions in the flow), these sediments accumulated in a flow-through lake; the presence of ground-wedge pseudomorphs in the underlying sediments is indicative of the probable thermokarst origin of this lake. Within the hollow section, the sandy sediments of layer 4 with inclined bedding layering are located in the area of permanent watercourses on the Passega diagram (Fig. 5).

The Sartan sediments (layers 5, 6) are identified on the ridges and in the hollow, under khasyreys. Layer 5 is represented by sands and loamy sands with *in situ* roots of herbs and sandy ground wedges. Layer 6 is represented by loamy sands with sand interlayers and with postcryogenic structures. Ground wedges (B14) were identified as pseudomorphs that substituted syncryogenic ice wedges (as judged from their internal structure and upward curved layers of the host sands. On the Passega diagram, these sands occupy the region of temporary watercourses and can be attributed to subaerial deluvial-proluvial (colluvial) deposits.

Within the hollow, layer 5 is composed of layered sands with interlayers and lenses of the washed in mosses and dwarfs shrubs; according to their position on the Passega diagram, these sediments accumulated in shallowing permanent watercourses. Layer 6 is represented by peaty loamy sands and silty sands and contain fine ground veins. On the Passega diagram, it is located in the zone of gradational suspensions from temporary to permanent watercourses. Taking into consideration the remains of sedges, *in situ* mosses, and washed-in detritus, this layer was attributed to sediments of flow-through shallowing water bodies (C3, C4, B7; Figs. 3, 4, 5). Sartan alluvial sediments of layer 5 date back to 21 500–17 800 BP with inversion of the dates, and lacustrine sediments of layer 6 date back to the Late Dryas (10 900–10 100 BP). The top of the Sartan sediments on the ridges was found at 28–32 m a.s.l.; in the hollow, at 4–5 m a.s.l.; the amplitude of heights is up to 23–27 m.

The Holocene sediments on the ridges are represented by layer 9 composed of slope sediments with developing bare circles and soil. In the khasyreys, the upper layer is composed of autochthonous peat, and it is subdivided into three layers differing in radiocarbon ages: 9.2–5.0 ka BP for layer 7, 4.0–2.7 ka BP for layer 8, and 1.6–0.8 ka BP for layer 9. The top of the Holocene sediments on the ridges is located at 33–28 m a.s.l.; in the khasyreys of the hollow, at 8–10 m a.s.l. The amplitude of heights is about 20–25 m.

#### Discussion of the formation of the III lacustrine-alluvial plain

The structures of sediment sections studied at different hypsometric levels of the III lacustrine-alluvial plain have both common features and significant differences.

The Lower Karginisk alluvial sediments with pseudomorphs developed in place of syncryogenic ice wedges were probably formed under conditions of leveled or flat landforms. Alluvial sands of layers 1, 2 on the ridges accumulated during the Early Karginisk warm period. They have no signs of thawing and are classified as epicryogenic. The sediments of flow-through lakes or floodplains with allochthonous detritus (layer 3) froze with the development of ice wedges probably during the Middle Karginisk (Lokhpodgortian) cooling [Arkhipov, Volkova, 1994] and thawed in the lake talik, so they are classified as taberal epicryogenic frozen sediments.

The Sartan sediments differ in the origin, accumulation conditions, and type of freezing. During the Sartan Glaciation, syncryogenic colluvium with ice wedges was formed on the ridges. Alluvium accumulated in the hollow over the eroded surface of the Lower Karginisk sediments. These sediments of permanent weak watercourses with redeposited Lower Sartan plant remains of good preservation degree and without visible signs of cyclic freezing–thawing were classified as epicryogenic. Erosion processes that occurred at the beginning of the Sartan period (before 17 800 BP) on the ridges and within the depressions were likely of low intensity, as they did not lead to the complete erosion of the Lower Karginisk sediments with pseudomorphs. The accumulation of alluvium in the hollow began after 17 ka BP, as evidenced by inversion of the radiocarbon ages in layer 5, which could take place because of the redeposition of first younger and then older sediments eroded from the ridges (Fig. 3 and Table 2). At the end of the Sartan epoch, about 11–10 ka BP, shallow overgrowing lakes existed in the hollow, which is indicated by the predominance of sedges in the peat. Thermal denudation and thawing could take place on the ridges, which is indirectly indicated by pseudomorphs. Alternation of freezing and thawing processes on the ridges led to the formation of taberal sediments with pseudomorphs and paleocryogenic deformations subjected

to secondary freezing; on the plains, under khasyreys, epicryogenic sediments were formed [Slagoda *et al.*, 2019]. These data suggest that taliks existed both on the uvalas and in the hollow under water bodies in the second half of the Sartan Cryochron.

The Holocene sediments in the hollow are represented by autochthonous peat of the khasyreys. Its accumulation in the center of the hollow began earlier (about 10 ka BP) than in their marginal parts near the ridges (9200–9100 BP). The predominance of sedges, hypnum mosses, and disappearance of dwarf birch in the peat were caused by fluctuations in the dry and warm and cold and wet conditions in the Boreal time [Arkhipov, Volkova, 1994]. Peat accumulated more actively about 8.6–8.0 ka BP: hypnum mosses grew on moistened polygons, sedges and cotton grass occupied waterlogged depressions, and willow shrubs and horsetails developed on the relatively drained sites (on the convex bends). The composition of peat in the Late Boreal period corresponded to relatively dry and warm conditions with excessive moistening in khasyreys. During the warm Atlantic period (about 7.7–5.4 ka BP), a larger part of the peat layer (2–3 m) was accumulated. Dwarf shrubs with mosses prevailed on less moistened high-center polygons, sedges developed in waterlogged depressions within polygons, and sphagnum mosses or herbaceous plants occupied interpolygonal depressions subjected to considerable fluctuations in the degree of moistening [Kuznetsova *et al.*, 2020].

The Late Holocene peat with a thickness of 0.1–0.5 m (layer 8) is locally present in khasyreys. In the Subboreal (4.0–2.7 ka BP), mosses, herbs, and dwarf shrubs grew under the cold and wet conditions. Peat of the active layer (layer 9) accumulated during the Subatlantic (1.6–0.1 ka BP); it consists of sphagnum, hypnum mosses, and sedges growing under the cold and relatively wet conditions.

The peatland in the hollow is a syncryogenic formation, because peat accumulation throughout the Holocene (since the Boreal time) was accompanied by freezing and growth of ice wedges. Partial melting of the ice wedges followed by resumption of their growth, as well as changes in the floristic composition of peat reflect changes in the moisture and heat supply against the background of climate fluctuations in the Holocene [Kuznetsova *et al.*, 2020; Tikhonravova *et al.*, 2023].

Correlation of the sections allowed us to trace the changes in the environment that contributed to the formation of the modern landforms in the northern part of the Pur–Taz interfluvium. The integrated section shows that the position of the upper bound varies within the amplitude of about 14–27 m for the Lower Karginsk sediments, 23–27 m for the Sartan sediments, and 20–25 m for the Holocene sediments. Probably, there was no such amplitude in the Early Karginsk time, when sediment accumulation and

growth of ice wedges took place on the floodplain and natural levees with approximately the same absolute heights. It is probable that the studied area in the Early Karginsk time represented a flat paleovalley oriented in agreement with the fault zones and modern contours of the low terraces of the Taz River (Fig. 1). The formation of the paleovalleys on Yamal, Gydan, and Taz Peninsulas is attributed to different times and causes. In the Early and Middle Neopleistocene, and in the Kazanian, the paleovalleys were associated with sea level lowering [Badu, 2011]; in the Late Sartan, with erosion activity of large rivers [Sidorchuk *et al.*, 2008]. In the Late Karginsk warming, thermokarst and thermal denudation developed [Arkhipov, Volkova, 1994], and the Middle and Upper Karginsk sediments were probably eroded.

According to our data, the relief of the paleovalley was reshaped in the Sartan epoch; apparently, due to differentiation of accumulative processes. On the ridges, slope syncryogenic sediments with ice wedges accumulated due to thermal erosion and material removal from higher ridges in the west and south of the area. The hollow began to be gradually filled with alluvium only in the second half of the Sartan epoch due to redeposition of the Lower Sartan sediments from the ridges. The preservation of pseudomorphs in the Sartan sediments of the ridges suggests the low intensity of thermal erosion because of low precipitation and the relatively resistant to erosion ice-bonded nature of permafrost.

In our opinion, the difference in heights of the Lower Karginsk and Sartan sediment sequences on the ridges and in the hollow and the preservation of the lower parts of pseudomorphs developed in place of ice wedges suggest that the reconstruction of the relief was related to the neotectonic descent of the hollow along the fractured zone of the north-northwestern strike that began about 17 ka BP. This process stopped and denudation of elevated landforms attenuated at the very beginning of the Holocene (or in final Dryas) between 11 ka and 10 ka BP. This is evidenced by the simultaneous accumulation of lacustrine sediments both in the erosion-neotectonic hollow and on the slopes of the ridges in thermokarst lakes. During this period, thawing of the Sartan permafrost with ice wedges and the formation of pseudomorphs could begin on slopes of the ridges. During relatively cold Preboreal and Boreal periods of the Holocene, sediments fixed by vegetation on the ridges were weakly affected by denudation.

During the Atlantic period, the thawing of permafrost with ice wedges and the formation of pseudomorphs probably continued on the ridges. In the hollow, the accumulation of polygonal peatlands was accompanied by their syngenetic freezing and growth of ice wedges, which corresponds to the concepts about the development of peat massifs in the north of Western Siberia [Vasil'chuk *et al.*, 2008]. The great

thickness of peat in the khasyreys is probably caused by the low activity of downward movements in the hollow along the fractured zone and by the weak erosional activity in the Holocene. In the Holocene Optimum, thermokarst development and melting of ice wedges could lead to the formation of lakes; their drainage in the Subboreal and Subatlantic could lead to waterlogging and growth of new ice wedges. Neotectonic movements probably continued along the fractured zone of the north-northeastern strike, where the valleys of small rivers were formed (Fig. 1).

Thus, these new data suggest that the local neotectonic processes that ended at the very beginning of the Holocene and the fluctuations of paleoclimatic conditions in the Holocene were important factors in the formation of the hollow-ridge landforms of the III lacustrine-alluvial plain of the Pur–Taz interfluvium starting from the second half of the Sartan epoch.

### CONCLUSION

Studies of the structure of the upper part of the III lacustrine-alluvial plain in the north of the Pur–Taz interfluvium made it possible:

1. To establish the cryogenic structure, lithological composition, and origin of permafrost on the ridges and in the hollows of the Pur–Taz interfluvium and to specify the floristic composition of peat and the conditions of its growth.

2. To identify the Lower Karginsk, Upper Sartan, and Holocene sediments according to the results of radiocarbon dating.

3. To attribute the Karginsk and Sartan horizons to the secondary epicryogenic tabular sediments with pseudomorphs on the ridges and to primary epicryogenic sediments in the hollows; the Holocene peat accumulated in the hollows was attributed to syncryogenic formations.

4. To correlate the sections of the upper part of permafrost on the slopes of the ridges and in the hollows and to establish that the absolute height of the upper boundary of the Lower Karginsk sediments with pseudomorphs along ice wedges varies with the amplitude of about 25 m and probably represents a fragment of the pre-Taz valley in this area. The Lower Karginsk sediments are overlain by the Sartan slope sediments with pseudomorphs on the ridges and by the Upper Sartan alluvial sediments in the hollows.

5. To substantiate the different altitudinal position of the Lower Karginsk sequence by the neotectonic subsidence of the hollow along the fractured zone of north-northeastern strike; this subsidence could continue from about 17 ka BP to 11 ka BP. The attenuation of neotectonic processes occurred in the Dryas (11 ka–10 ka BP) and was recorded in the formation of thermokarst lakes in the hollow.

6. To reveal the influence of the Holocene paleoclimatic conditions on the differentiated develop-

ment of relief-forming processes: thermal denudation and melting of ice wedges with the formation of pseudomorphs occurred on the ridges; freezing processes and growth of ice wedges continued in the hollows.

**Acknowledgments.** This work was carried out within the framework of state assignment of the Ministry of Science and Higher Education of the Russian Federation to the Institute of Earth Cryosphere, Tyumen Scientific Center, Siberian Branch, Russian Academy of Sciences (theme no. FWRZ-2021-0012).

### References

- Andreev Yu.F., 1960. On the connection of the linear-ridge relief with tectonic structures in the north of Western Siberia in the area of permafrost development. *Geol. Geokhim.* 3 (IX), 76–94. (in Russian)
- Arkipov S.A., Volkova V.S., 1994. *Geological History, Pleistocene Landscapes and Climate in West Siberia*. Novosibirsk, NITS OIGGM SO RAN, 105 p. (in Russian)
- Arkipov S.A., Levchuk L.K., Shelkopyas V.N., 1994. Stratigraphy and geological structure of the Quaternary cover of Lower-Ob–Yamal–Taz region in West Siberia. *Russ. Geol. Geofizika* 35 (6), 87–104. (in Russian)
- Astakhov V.I., 2009. Middle and Late Neopleistocene of the glacial zone of Western Siberia: problems of stratigraphy and paleogeography. *Byull. Komm. Izuch. Chetvertich. Perioda* 69, 8–24. (in Russian)
- Babkina E.A., Khomutov A.V., Babkin E.M., Leibman M.O., 2022. Monitoring of active layer depth and permafrost temperature in the north of Yamal–Nenets AD. In: *Relief and Quaternary Deposits of the Arctic, Subarctic and Northwest Russia*. Proc. Annual Conf. on the Results of Expeditionary Research, no. 9. St. Petersburg, VNIIOkeangeologia, p. 20–28. (in Russian)
- Badu Yu.B., 2011. Geology of cryogenic strata in the northern part of Western Siberia. *Inzhener. Geol.* 1, 40–55. (in Russian)
- Bragin P.E., 2001. Problems of neotectonics of the West Siberian lowland. *Ural'sk. Geol. Zh.* 1, 69–82. (in Russian)
- Decision of the 6th Interdepartmental Stratigraphic Meeting on the Review and Adoption of Updated Stratigraphic Schemes of Mesozoic Deposits in Western Siberia*, 2004. Novosibirsk, SNIIGGiMS, 114 p. (in Russian)
- Ershov E.D. (Ed.), 1989. *Geocryology of the USSR. Vol. 2. Western Siberia*. Moscow, Nedra, 454 p. (in Russian)
- Filippovich Yu.V., 2012. *Strike-Slip Tectonics in the Area of the Nadym–Taz Interfluvium and Methods for Forecasting Oil Deposits*. Author's Abstract Cand. Sci. (Geol.–Mineral.) Dissertation. Moscow, 20 p. (in Russian)
- Gorodetskaya M.E., 1972. The main morphostructural lineaments and the cycles in the relief development of the West Siberian Plain. *Geomorfologiya* 4, 33–42. (in Russian)
- Grosswald M.G., 1983. *Ice Sheets of Continental Shelves*. Moscow, Nedra, 216 p. (in Russian)
- Gusev E.A., 2015. Cenozoic sediment cover neotectonic deformations in the Yenisei Bay area (Kara Sea). *Arktich. Antarktich. Issled.* 3 (105), 5–14. (in Russian)
- Hua Q., Barbetti M., Rakowski A., 2013. Atmospheric radiocarbon for the period 1950–2010. *Radiocarbon* 55 (4), 2059–2072.
- Kaplina T.N., 2009. Alas complex of northern Yakutia. *Kriosfera Zemli* XIII (4), 3–17. (in Russian)

- Katasonov E.M., 2009. *Lithology of Frozen Quaternary Deposits (Cryolithology) of the Yanskaya Primorsky Lowland*. Moscow, OAO PNIIS, 176 p. (in Russian).
- Khomutov A.V., Babkin E.M., Tikhonravova Ya.V. et al., 2019. Integrated studies of the cryolithozone in the northeastern part of the Pur–Taz interfluvium. *Nauchn. Vestn. Yamalo-Nenetsk. Avtonomn. Okruga* (Salekhard) 1 (102), 53–64. (in Russian)
- Khotinsky N.A., 1977. *Holocene of Northern Eurasia*. Moscow, Nauka, 198 p. (in Russian)
- Koroleva E.S., 2022. *Development of Permafrost Polygonal Peatlands under the Influence of Changes in the Environmental Conditions of the Pur–Taz Interfluvium in Western Siberia*. Author's abstract Cand Sci. (Geol.-Mineral.) dissertation. Tyumen, 22 p. (in Russian)
- Kuzin I.L., 2005. *Geomorphology of the West Siberian Plain*. St. Petersburg, Izd. Gos. Polyarn. Akad., 176 p. (in Russian)
- Kuznetsova A.O., Slagoda E.A., Koroleva E.S., Tikhonravova Y.V., 2022. Reconstruction of local natural conditions of peat accumulation during the Holocene period of the southern hypoarctic tundra of the Pur–Taz interfluvium. In: *Proc. Sixth Russian. Conf. Geocryolog.* Moscow, KDU, Dobrovset, p. 1062–1069. (in Russian)
- Kuznetsova A.O., Tikhonravova Ya.V., Slagoda E.A., Afonin A.A., 2020. Holocene dynamics of local conditions of peat formation in the Arctic zone of Western Siberia. In: *Global Problems of the Arctic and Antarctic*. Materials of the All-Russia Conf. with Int. Participation. Arkhangelsk, FITSKIA UrO RAN, p. 122–125. (in Russian)
- Manuilova E.A., 2021. The latest structural plan of the West Siberian Plate. *Vestn. Mosk. Gos. Univ., Ser. 4: Geol.* 76 (1), 23–30. (in Russian)
- Melnikov E.S., Moskalenko N.G. (Ed.), 1991. *Map of Natural Systems in the North of Western Siberia for Geocryological Forecasting and Planning Environmental Measures during Mass Construction (Scale 1 : 1,000,000)*. Moscow, VSEGIN-GEO, 6 p. (in Russian)
- Nazarov D.V., 2015. Upper Pleistocene of the north of Western Siberia. In: *Proc. IX Russian Meeting on the Study of the Quaternary Period*. Irkutsk, Izd. Inst. Geogr. i im. V.B. Sochavy SO RAN, p. 323–325. (in Russian)
- Pozdnyakov A.V., Puchkin A.V., Pupyshev Yu.S. et al., 2020. Genesis of the ridge-hollow relief of the West Siberian Plain. *Geosfer. Issled.* 4, 42–57. (in Russian)
- Reinek H.-E., Singh I.B., 1975. *Depositional Sedimentary Environments*. Berlin, Heidelberg, New York, Springer-Verlag, 439 p.
- Savchenko N.V., 2016. Paleogeographic and geology-geomorphology factors of geomorphology of the Western Siberia. *Sci. Europe. Geograph. Sci.* 9 (9), 4–12. (in Russian)
- Sidorchuk A.Yu., Panin A.V., Borisova O.K., 2008. Late glacial palaeochannels in West Siberia. *Izv. Ross. Akad. Nauk. Geogr.* 2, 67–75. (in Russian)
- Slagoda E.A., Balandin V.A., Oshchepkova E.B., 2001. Permafrost phenomena as an indicator of the course of neotectonic processes. Abstracts Conf. Dedicated to the 90th Anniversary of the Birth of Acad. A.L. Yanshin. Novosibirsk, Acad. Publ. House “Geo”, p. 61. (in Russian)
- Slagoda E.A., Medvedev G.I., 2004. Paleocryogenic formation, stratigraphy and geoarcheology of the Quaternary deposits of Baikal's Siberia. *Kriosfera Zemli* VIII (1), 18–28. (in Russian)
- Slagoda E.A., Novoselov A.A., Koroleva E.S. et al., 2022. Traces of cryogenic processes in the late Pleistocene sediments of the Pur–Taz interfluvium (West Siberia). *Earth's Cryosphere* XXVI (1), 19–31.
- Slagoda E.A., Opokina O.L., Popov K.A., Orekhov P.T., 2015. To the reconstruction of cryogenic and seismic issues. In: *Proc. IX Russian Meeting on the Study of the Quaternary Period*. Irkutsk, Izd. Inst. Geogr. im. V.B. Sochavy SO RAN, p. 435–437. (in Russian)
- Slagoda E.A., Tikhonravova Ya.V., Kuznetsova A.O., Koroleva E.S., 2019. Cryoturbations, pseudomorphs, postcryogenic structures and involutions in the frozen sediments of the Pur–Taz interfluvium. Solving the Puzzles from Cryosphere: Abstracts Int. Conf. Pushchino, Okabiolab Ltd, p. 109–110.
- Stuiver M., Reimer P.J., 1993. Extended <sup>14</sup>C database and revised CALIB radiocarbon calibration program. *Radiocarbon* 35, 215–230.
- Tikhonravova Y., Kuznetsova A., Slagoda E., Koroleva E., 2023. Holocene permafrost peatland evolution in drained lake basins on the Pur–Taz Interfluvium, North-Western Siberia. *Quat. Int.* 669, 32–42.
- Tikhonravova Ya.V., Slagoda E.A., Rogov V.V. et al., 2020. Heterogeneous structure of polygonal wedge ice in the peat bogs of the Pur–Taz interfluvium. *Led i Sneg* 60 (2), 225–238. (in Russian)
- Trofimov V.T., Badu Yu.B., Vasilchuk Yu.K. et al., 1987. *Geocryological Zoning of the West Siberian Plate*. Moscow, Nauka, 219 p. (in Russian)
- Tumskoy V.E., 2021. Cryolithostratigraphy and cryofacies analysis. *Earth's Cryosphere* XXV (4), 3–13.
- Vasil'chuk Yu.K., Vasil'chuk A.C., Budantseva N.A. et al., 2008. *Convex Frost Mounds of Permafrost Peat Massifs*. Moscow, Moscow Univ. Press, 571 p. (in Russian)
- Vasil'chuk Yu.K., Vasil'chuk A.C., 2016. Thick polygonal peatlands in continuous permafrost zone of Western Siberia. *Earth's Cryosphere* XX (4), 3–13.
- Velichko A.A., Faustova M.A., Pisareva V.V., Karpukhina N.V., 2017. History of the Scandinavian ice sheet and surrounding landscapes in the Valday ice age and the Early Holocene. *Led i Sneg* 57 (3), 391–416. (in Russian)
- Zazovskaya E.P., 2016. Radiocarbon dating – modern state, problem, prospects of development and use in archaeology. *Vestn. Arkheolog. Antropolog. Etnografii* 1 (32), 151–164. (in Russian)
- Zhamoyda A.I. (Ed.), 2019. *Stratigraphic Code of Russia*. Third edition, corrected and enlarged. St. Petersburg, Izd. VSEGEI, 96 p. (in Russian).
- Zykina V.S., Zykin V.S., Volvach A.O. et al., 2017. Upper Quaternary deposits of the Nadym Ob area: stratigraphy, cryogenic formations, and deposition environments. *Earth's Cryosphere* XXI (6), 12–20.

Received August 30, 2023

Revised March 7, 2024

Accepted April 6, 2024

Translated by V.A. Krutikova